J. Fluid Mech. (2001), *vol.* 445, *pp.* 37–54. © 2001 Cambridge University Press
DOI: 10.1017/S0022112001005444 Printed in the United Kingdom

Theory for producing a single-phase rarefaction shock wave in a shock tube

By S. H. FERGASON[1], T. L. HO[2], B. M. ARGROW[1] AND G. EMANUEL[3]

[1]University of Colorado, Boulder, CO 80309, USA
[2]University of Oklahoma, Norman, OK 73019, USA
[3]University of Texas, Arlington, TX 76019, USA

(Received 4 August 2000 and in revised form 23 April 2001)

Although predicted early in the 20th century, a single-phase vapour rarefaction shock wave has yet to be demonstrated experimentally. Results from a previous shock tube experiment appear to indicate a rarefaction shock wave. These results are discussed and their interpretation challenged. In preparation for a new shock tube experiment, a global theory is developed, utilizing a van der Waals fluid, for demonstrating a single-phase vapour rarefaction shock wave in the incident flow of the shock tube. The flow consists of four uniform regions separated by three constant-speed discontinuities: a rarefaction shock, a compression shock, and a contact surface. Entropy jumps and upstream supersonic Mach number conditions are verified for both shock waves. The conceptual van der Waals model is applied to the fluid perfluoro-tripentylamine (FC-70, $C_{15}F_{33}N$) analytically, and verified with computational simulations. The analysis predicts a small region of initial states that may be used to unequivocally demonstrate the existence of a single-phase vapour rarefaction shock wave. Simulation results in the form of representative sets of thermodynamic state data (pressure, density, Mach number, and fundamental derivative of gas dynamics) are presented.

1. Introduction

Rarefaction shock waves (RSW), and related non-classical phenomena, have been frequently addressed in this journal. The cited references contain a non-exhaustive list of *JFM* papers with analyses that indicate the possibility of sonic shocks (Cramer & Sen 1986, 1987), split shocks (Cramer 1989; Cramer & Sen 1990; Cramer 1991), etc., in a pure single-phase vapour. When it was realized that single-phase vapour non-classical phenomena are probably possible and possibly useful (e.g. Brown & Argrow 1998, 2000), theoretical efforts produced a general description of the characteristics of non-classical wave fields. This theoretical treatment focused primarily on simple idealized flow fields and with the exception of the two-phase studies of P. A. Thompson's group (Thompson & Kim 1983; Thompson, Carofano & Kim 1986), analytical and computational studies have not adequately assessed how these features might be investigated in an experimental device, such as a shock tube (Argrow 1996; Brown & Argrow 1997).

Despite these analytical and computational studies, experimental confirmation of the single most important non-classical feature – a RSW, still does not exist. A possible exception is the experiment of Borisov *et al.* (1983), where a single-phase vapour RSW

https://doi.org/10.1017/S0022112001005444 Published online by Cambridge University Press

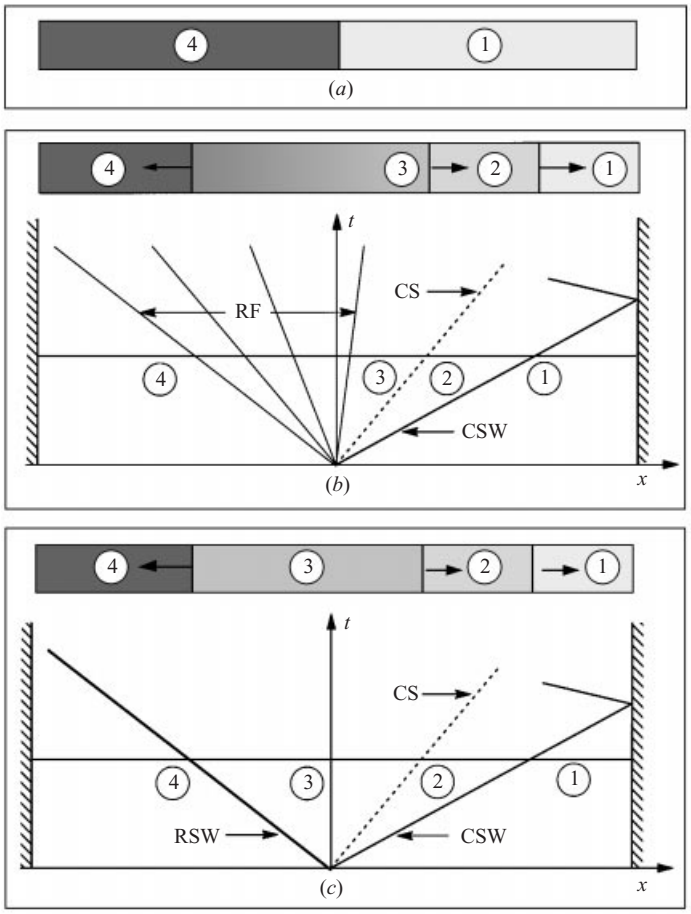


FIGURE 1. Shock tube wave field schematic.

is said to be demonstrated. In the next section, this assertion is re-evaluated. Related vapour-phase features, such as a double sonic shock, are similarly unconfirmed.

We have begun an experimental study of non-classical dense gas dynamics at the University of Colorado, Boulder. A shock tube has been constructed to generate a vapour-phase RSW in the incident wave field. A primary difficulty, in our view, is the lack of a global theory that gives a systematic approach for consistent initial conditions. This paper provides a theory with supporting analysis. The focus is on the most feasible experimental case, i.e. an incident shock tube flow that contains no fans or split waves, but only three distinct discontinuities. This choice is made based upon the need to produce the maximum strength RSW for experimental measurement.

Figure 1 illustrates the initial and dynamic states of the incident, inviscid wave field. Figure 1(*a*) shows the shock tube initial condition with the darker-shaded state 4 the high pressure and density state, and the lighter-shaded state 1 the low pressure and density state. The graduated shading in figure 1 illustrates the variation of the density field. The wave fields are projected onto x, t diagrams where the instant in time t is marked by the horizontal line. Figure 1(*b*) illustrates the classical wave field of a perfect gas, where the head of a rarefaction fan (RF) propagates into the quiescent, high-density state 4 and a compression shock wave (CSW) propagates into the low-

https://doi.org/10.1017/S0022112001005444 Published online by Cambridge University Press

density state 1. In figure 1(*b*) states 2 and 3 respectively refer to the conditions immediately downstream of the CSW and the contact surface (CS). Note the smooth density decrease through the RF connecting states 4 and 3. The non-classical triple-discontinuity wave field of a fluid displaying negative nonlinearity is illustrated in figure 1(*c*). The RF has coalesced into a RSW and there is a uniform density value, state 3, between the RSW and CS.

The following global analysis does not address the totality of shock tube flows that might contain a RSW. By focusing on the incident flow, various complicating interactions are avoided, such as an interaction of a wave with an upstream boundary layer. Moreover, if a triple-discontinuity wave field can be established, its experimental verification is straightforward and its physical interpretation is unambiguous. Three assumptions, based on the experimental design, are introduced to facilitate computation of the triple-discontinuity solution. First, both sides of the tube are assumed to have the same initial temperature, since a uniform initial temperature is easier to control and there is no apparent experimental advantage otherwise. Second, the same fluid is assumed on both sides of the diaphragm. A preliminary analysis that examined the possibility of using different driver and driven fluids proved unproductive. The final assumption of a van der Waals (VDW) fluid introduces a relatively simple equation of state (EOS). Although the VDW model is not particularly accurate, its analytical simplicity for this type of study is unmatched. Later, the more realistic, but more complex Martin–Hou (Martin & Hou 1955, 1959) (MH) EOS is used. Computational fluid dynamics results employing both the VDW EOS and the MH EOS are also presented. The chosen fluid must possess a relatively large value for the ratio c_v/R, where c_v is the specific heat at constant volume and R is the specific gas constant. This requires a gas molecule with a large number of atoms and a correspondingly large molecular weight. The magnitude of c_v/R required for the gas model to display negative nonlinearity and support a RSW depends upon the EOS. This is discussed later.

The present study addresses a number of dense gas flow issues, starting with the existence of a triple-discontinuity solution. If this solution exists, can it be realistically demonstrated in a shock tube experiment? What is an appropriate fluid for this demonstration, and which uniform flow states require a negative value for the fundamental derivative of gas dynamics? These are some of the questions addressed.

The next section re-examines the experiment of Borisov *et al.* (1983). Section 3 contains the global analytical model and provides results for perfluoro-tripentylamine (FC-70, $C_{15}F_{33}N$). The computational model and simulation results are presented in § 4 and § 5. The paper concludes with a summary discussion.

2. Previous experimental results

In the Borisov *et al.* (1983) experiment, a specially designed shock tube was used with trifluorochloromethane (F-13, $CClF_3$) in which the initial state of the fluid in the high-pressure side of the tube was evidently close to the critical point. After the diaphragm was ruptured, a dispersed wave of about 3 cm thickness propagated into the fluid on the high-pressure side with little or no change in profile. It was asserted that this was a single-phase RSW and this assertion is restated in Kutateladze, Nakoryakov & Borisov (1987).

The interpretation of the data collected in the Borisov *et al.* (1983) experiment can be questioned based on thermodynamic arguments and Euler simulations. First, the choice of fluid is not consistent with the requirements of Thompson & Lambrakis

https://doi.org/10.1017/S0022112001005444 Published online by Cambridge University Press

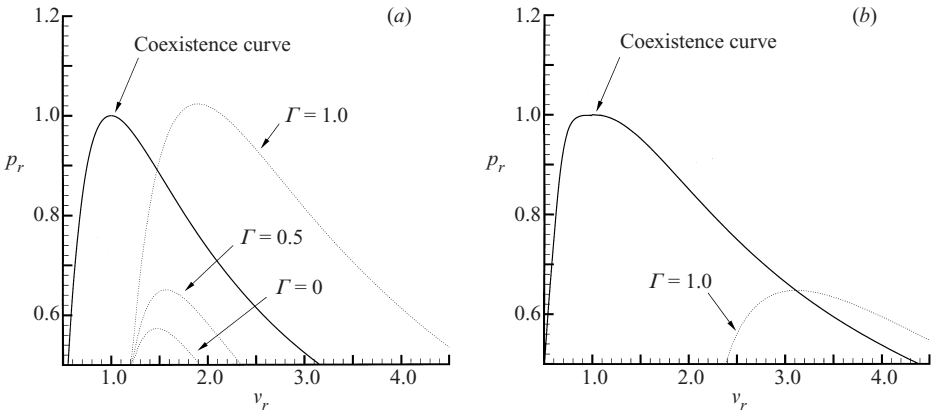


FIGURE 2. Iso-Γ lines for F-13, (*a*) VDW and (*b*) MH EOS.

(1973) for negative nonlinearity. The fundamental derivative of gas dynamics,

$$\Gamma = 1 - \frac{v}{a}\left(\frac{\partial a}{\partial v}\right)_s, \tag{2.1}$$

is the principal parameter associated with negative nonlinearity and non-classical behaviour, where v is the specific volume, a is the speed of sound, and s is the entropy. Positive and negative nonlinearity are associated with a respective positive or negative Γ-value. For a perfect gas $\Gamma = (\gamma + 1)/2$, where γ is the ratio of specific heats and Γ exceeds unity; the perfect gas always exhibits positive nonlinearity. When the magnitude of Γ is near zero a dispersed wave propagates with little or no discernible change in its profile (Thompson 1988).

Figures 2(*a*) and 2(*b*) are pressure p_r vs. specific volume v_r diagrams for F-13 using the VDW and MH EOS, where the r subscript indicates reduced variables. The Γ-contours of both EOS models indicate that F-13 cannot produce a single-phase vapour state with a negative-Γ value. It should be noted that due to the non-analytical behaviour of all fluids at a critical point, any classical EOS, including the MH EOS, is not accurate very near the liquid–vapour critical point. Nevertheless, both figures indicate qualitative behaviour.

Retrograde behaviour is exhibited by real fluids with high heat capacity (large values of c_v/R) whose vapours tend to condense on adiabatic compression. This contrasts with the *regular behaviour* of fluids with lower heat capacity, such as water, which tend to condense on adiabatic expansion (Thompson *et al.* 1986). The thermodynamic requirement for retrograde behaviour is that the derivative of the entropy with respect to the temperature along the vapour side of the coexistence curve is positive (i.e. $\mathrm{d}s_g/\mathrm{d}T > 0$). For real fluids the c_v/R value required for the onset of retrograde behaviour is lower than that for the onset of negative nonlinearity in the vapour phase (Thompson *et al.* 1986). This means that for a real fluid to exhibit negative nonlinearity in the vapour phase it must also exhibit retrograde behaviour. Using a thermodynamic table (e.g. Stewart, Jacobsen & Penocello 1969) one can demonstrate that F-13 is not a retrograde fluid – thus it cannot exhibit negative nonlinearity in the pure vapour phase. On a thermodynamic basis, it appears impossible that F-13 can exhibit any non-classical behaviour in the pure vapour phase, including a RSW.

An Euler simulation of the experiment was performed using initial conditions reported in Borisov *et al.* (1983). Figure 3 shows the p_r, v_r data, critical isentrope, and

https://doi.org/10.1017/S0022112001005444 Published online by Cambridge University Press

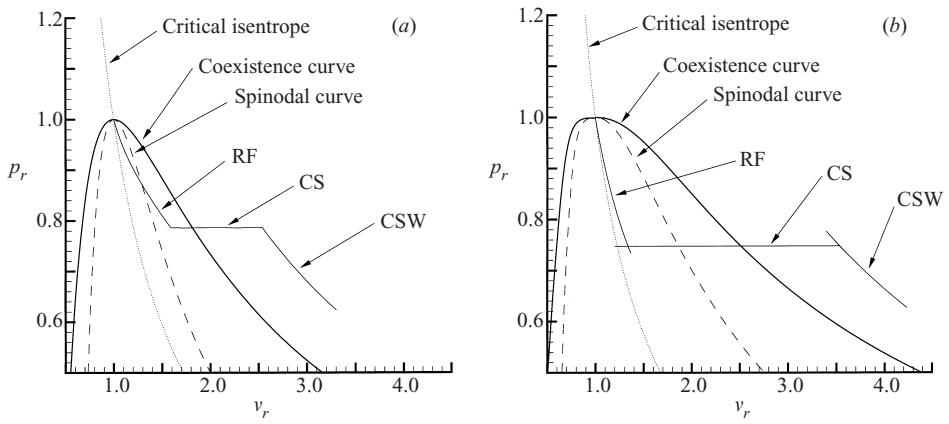


FIGURE 3. Coexistence curve, spinodal curve, and critical isentrope for F-13 with simulated $p_r - v_r$ data using (*a*) the VDW and (*b*) MH EOS.

coexistence and spinodal curves using both the VDW and MH EOS. In each case, a portion, or all, of the rarefaction wave lies beneath the spinodal curve. This indicates the wave must contain two-phase liquid states. Our computational model has no provisions for simulating two-phase flow states, making the results only qualitative. In figure 3(*b*) the overshoots in the solution at the intersections of the RF and CSW states with the CS states are numerical artifacts. The simulations shown in figure 3 were computed with the same algorithm and same level of discretization as the simulations discussed in more detail in § 5.

Thompson (1991), Kutateladze *et al.* (1987), and Cramer & Sen (1986) all suggest that the wave profile may be associated with critical point phenomena due to the asymptotic increase of the specific heat at constant volume, where $c_v \to +\infty$ following the near-critical power law

$$c_v \propto [(T - T_c)/T_c]^{-\alpha}, \tag{2.2}$$

where α is the critical exponent (≈ 0.1). The important parameter, however, is not c_v but Γ, which becomes positively infinite as the critical point is approached from any direction in the vapour region (Emanuel 1996). Consequently, the initial high-pressure state may not have been as close to the critical point as expected. Alternatively, the shock adiabat that passes through the critical point falls inside the spinodal curve and the flow would not be single phase.

The cumulative weight of evidence suggests that the Borisov *et al.* (1983) experiment did not produce a single-phase RSW.

3. Analytical model

In preparation for our experimental study, a systematic approach for generating experimental initial conditions for the shock tube is required. Since any RSW is necessarily weak, emphasis must be placed on producing the maximum-strength wave. As previously stated, design considerations for the apparatus and relevance of the analytical model suggest a uniform initial temperature throughout the entire tube with the same fluid for both the driver and driven sections. The algorithm for analytically determining the initial and stationary states of the shock tube wave field is developed using the VDW EOS with results for the MH EOS also included.

Relevant thermodynamic equations for a VDW fluid (Emanuel 1997) are summar-

https://doi.org/10.1017/S0022112001005444 Published online by Cambridge University Press

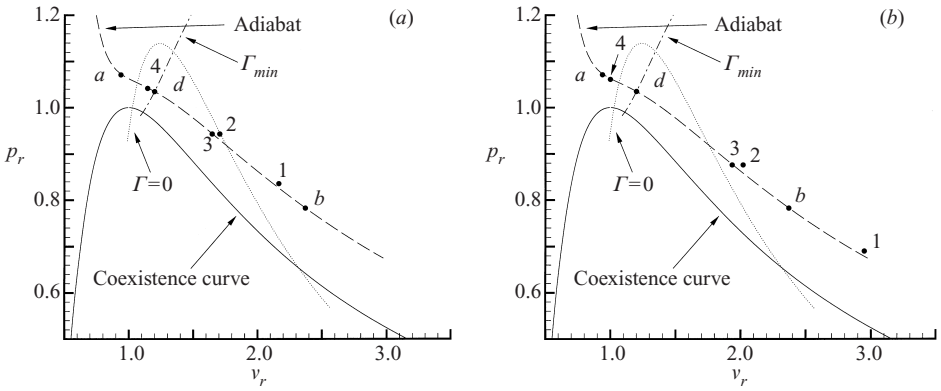


FIGURE 4. p_r, v_r diagrams showing the coexistence curve, $\Gamma = 0$ contour, Γ_{min} curve, and the respective states for cases (*a*) VDW1 and (*b*) VDW2. The state-*d* adiabat passes through states *a*, *b*, and 4.

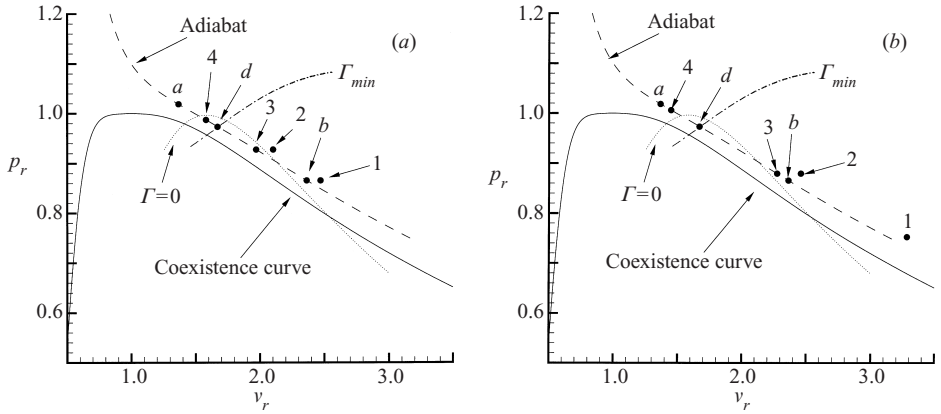


FIGURE 5. p_r, v_r diagrams showing the coexistence curve, $\Gamma = 0$ contour, Γ_{min} curve, and the respective states for cases (*a*) MH1 and (*b*) MH2. The state-*d* adiabat passes through states *a*, *b*, and 4.

ized in the Appendix. A c subscript denotes a critical-point value, an r subscript denotes a reduced variable, an overbar denotes a dimensional quantity, and f and g subscripts respectively denote the liquid and vapour sides of the coexistence curve (see (A 7) and (A 8) in the Appendix). It is assumed that m ($= c_v/R$) is a constant. Since the initial states have the same temperature and both shock waves are nearly isothermal, the constant-c_v assumption does not introduce significant error.

Figures 4 and 5 show the coexistence curve, the $\Gamma = 0$ curve, an adiabat, and several other features that will be discussed later for FC-70 ($m = 118.7$). The VDW EOS was used to produce figure 4 and the MH EOS was used for figure 5. Near the critical point the MH coexistence curve is flatter, in better accord with coexistence curves based on experimental data. Because of the overall similarity and relatively simple closed-form expressions, it is appropriate to discuss the VDW topology.

For a sufficiently large value of m, the VDW $\Gamma = 0$ curve is

$$T_r = \frac{m^2}{4(m+1)(2m+1)} \frac{(3v_r - 1)^3}{v_r^4}. \tag{3.1}$$

https://doi.org/10.1017/S0022112001005444 Published online by Cambridge University Press

Along a single-phase isentrope, Γ has a minimum value. This value is negative if it occurs inside the $\Gamma = 0$ contour. The equation for this Γ_{min} curve is (Emanuel 1997)

$$T_r = \frac{(3v_r - 1)^2[3(m-1)^2 v_r^2 + m(7-4m)v_r + 3m^2]}{4(m+1)(2m+1)v_r^4}, \tag{3.2}$$

and the value for Γ on this curve is

$$\Gamma_{min} = \frac{2m+1}{2m}\frac{3(m-1)v_r - 4m}{(m-1)v_r - m}\frac{v_r}{3v_r - 1}. \tag{3.3}$$

The Γ_{min} curve intersects the coexistence curve near the critical point and has its most negative single-phase value at this state.

The first step in the global procedure is to choose a state point d that is on the Γ_{min} curve, where Γ is negative, and to the right of the coexistence curve (see figure 4). A shock adiabat that passes through state d is constructed according to

$$h_r - h_{rd} = 3(p_r - p_{rd})(v_r + v_{rd})/16, \tag{3.4}$$

where h and p are enthalpy and pressure. Because of the location of state d, a portion of the adiabat through this state must be inside the negative-Γ region. For analytical convenience this relation is rewritten as

$$p_r = N/D, \tag{3.5}$$

where

$$N(v_r; m, h_{rd}, v_{rd}, p_{rd}) = 16m - 12 + 16h_{rd} - \frac{18(m-1)v_r - 6m}{v_r^2} - 3(v_r + v_{rd})p_{rd}, \tag{3.6}$$

$$D(v_r; m, v_{rd}) = 3(2m+1)v_r - (3v_{rd} + 2m). \tag{3.7}$$

When m is sufficiently large ($m > 16.7$ for the VDW EOS) the adiabat may have two inflection points in the vapour region and the $\Gamma = 0$ curve passes through these points. Outside of these inflection points are two state points, a and b, where a straight line (a Rayleigh line) through them is tangent to the adiabat at these points, as illustrated in figure 6. For clarity, the curvature of the adiabats is exaggerated in the figure. Observe that states a and b are uniquely defined in terms of m, p_r, and v_r, and that Γ_a and Γ_b are positive; indeed, Γ_a is generally well in excess of zero. Since the Rayleigh line is tangent to the adiabat at states a and b, the slope of the adiabat at these two points is the slope of the straight Rayleigh line. This gives the two conditions that define states a and b and determine v_{ra} and v_{rb},

$$\left(\frac{1}{D}\frac{\mathrm{d}N}{\mathrm{d}v_r} - \frac{N}{D^2}\frac{\mathrm{d}D}{\mathrm{d}v_r}\right)_{v_r = v_{ra}} = \left(\frac{1}{D}\frac{\mathrm{d}N}{\mathrm{d}v_r} - \frac{N}{D^2}\frac{\mathrm{d}D}{\mathrm{d}v_r}\right)_{v_r = v_{rb}}, \tag{3.8}$$

$$(v_{ra} - v_{rb})\left(\frac{1}{D}\frac{\mathrm{d}N}{\mathrm{d}v_r} - \frac{N}{D^2}\frac{\mathrm{d}D}{\mathrm{d}v_r}\right)_{v_r = v_{ra}} = \frac{N(v_{ra})}{D(v_{ra})} - \frac{N(v_{rb})}{D(v_{rb})}, \tag{3.9}$$

where $v_{rb} > v_{rd} > v_{ra}$.

The only function of states a and b is as convenient reference states and bounds for states 4 and 3, which are the upstream and downstream states for the disturbance in the high-pressure region. The specific volume at these states is defined in terms of v_{ra} and v_{rb} as

$$v_{r3} = v_{rb} - \delta_3(v_{rb} - v_{ra}), \quad v_{r4} = v_{ra} + \delta_4(v_{rb} - v_{ra}), \tag{3.10}$$

where δ_3 and δ_4 are prescribed non-negative parameters. State 4 is chosen as the

https://doi.org/10.1017/S0022112001005444 Published online by Cambridge University Press

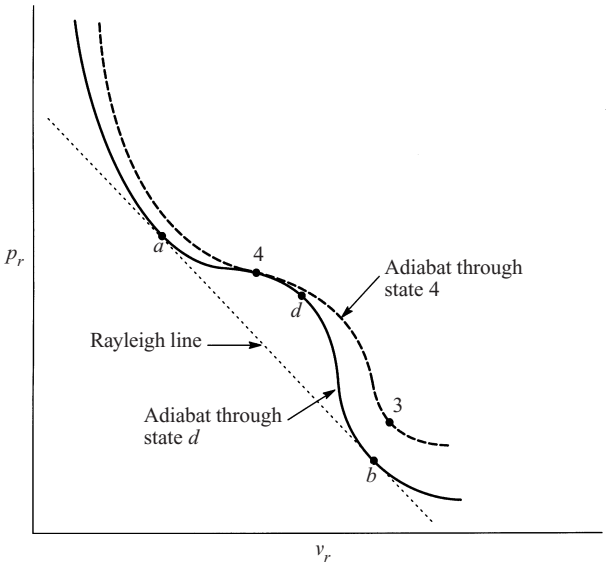


FIGURE 6. p_r, v_r schematic showing states a, b, d, and 4 on the adiabat through state d. States 3 and 4 lie on the adiabat through state 4. States a and b are connected by a Rayleigh line.

upstream state on the adiabat through state d,

$$h_{r4} - h_{rd} = 3(p_{r4} - p_{rd})(v_{r4} + v_{rd})/16, \tag{3.11}$$

whereas state 3 is on a different adiabat through state 4, referred to as adiabat 4–3,

$$h_{r3} - h_{r4} = 3(p_{r3} - p_{r4})(v_{r3} + v_{r4})/16. \tag{3.12}$$

We can eliminate h_{r4} from the previous two equations to obtain

$$h_{r3} - h_{rd} = 3[p_{r3}(v_{r3} + v_{r4}) + p_{r4}(v_{rd} - v_{r3}) - p_{rd}(v_{rd} + v_{r4})]/16, \tag{3.13}$$

which is *not* an adiabat connecting states d and 3. Thus, as sketched in figure 6, state 3 is not on the state-d adiabat. The adiabat with state 3, adiabat 4-3, is very close to the one through state d; it is not shown in figures 4 and 5. Thus, p_{r4} is determined by (3.5), whereas p_{r3} requires that the d subscript be replaced with a 4 in this equation. States a and b correspond to a double sonic shock. In the limit when $\delta_3 = \delta_4 = 0$, state 4 becomes state a but state 3 does not become state b, although it is very close to this state. Specification of v_{rd}, δ_3, and δ_4 thermodynamically fixes states a, b, d, 3, and 4. As will be evident, states 1 and 2 are also fixed.

Mass and momentum conservation provide the shock speed u_4 and flow speed for state 3, in a laboratory reference frame,

$$u_4 = -v_{r4}\left(\frac{3RT_c}{8}\frac{p_{r4} - p_{r3}}{v_{r3} - v_{r4}}\right)^{1/2}, \quad u_3 = \left(1 - \frac{v_{r3}}{v_{r4}}\right)u_4. \tag{3.14}$$

The corresponding Mach numbers, in a shock-fixed frame, are

$$M_4 = -\frac{u_4}{a_c a_{r4}}, \quad M_3 = \frac{u_3 - u_4}{a_c a_{r3}}, \tag{3.15}$$

where the Appendix provides equations for a_c and a_r. The CS and initial conditions are imposed, i.e.

$$u_2 = u_3, \quad p_{r2} = p_{r3}, \quad T_{r1} = T_{r4}. \tag{3.16}$$

https://doi.org/10.1017/S0022112001005444 Published online by Cambridge University Press

Case	State	p_r	v_r	Γ	M
VDW1	1	0.8355	2.1658	0.3505	1.0291
	2	0.9431	1.7064	0.0109	0.9843
	3	0.9431	1.6474	−0.1476	0.9251
	4	1.0417	1.1464	−0.9630	1.0106
VDW2	1	0.6898	2.9506	0.6112	1.1008
	2	0.8758	2.0200	0.2827	0.9218
	3	0.8758	1.9358	0.1715	0.9314
	4	1.0608	1.0000	1.7728	1.1780

TABLE 1. Shock tube conditions for cases VDW1 and VDW2 for $v_{rd} = 1.20$.

The shock jump conditions then result in

$$v_{r2} - v_{r1} + \frac{8}{3RT_c}\frac{u_2^2}{p_{r2} - p_{r1}} = 0, \tag{3.17}$$

$$\frac{9}{4}\frac{v_{r1} - v_{r2}}{v_{r1}v_{r2}} + \left(\frac{3v_{r1}}{3v_{r1} - 1} + m\right) T_{r1} - \frac{3v_{r2} - 1}{8}\left(p_{r2} + \frac{3}{v_{r2}^2}\right)\left(\frac{3v_{r2}}{3v_{r2} - 1} + m\right) + \frac{u_2^2}{2RT_c}\frac{v_{r1} + v_{r2}}{v_{r1} - v_{r2}} = 0, \tag{3.18}$$

for states 1 and 2. The unknowns are v_{r1} and v_{r2}, where, for a compressive shock wave, $v_{r1} > v_{r2}$. Once these are found, other parameters are easily determined, since u_2, p_{r2}, and T_{r1} are also known. For instance, the compressive shock speed and Mach number are given by

$$u_1 = \frac{u_2}{1 - v_{r2}/v_{r1}}, \quad M_1 = \frac{u_1}{a_c a_{r1}}. \tag{3.19}$$

Van der Waals modelling of a variety of fluids, including FC-70, provides several general conclusions. For values of v_{rd} below about 1.1, state 4 is in the two-phase mixture region and relatively close to the critical point. On the other hand, the Γ_{min} and $\Gamma = 0$ curves cross when (Emanuel 1997)

$$v_{rd}^* = \frac{4m}{3(m-1)}. \tag{3.20}$$

At this v_{rd} value, states a, b, and d coincide. Thus, there is a relatively narrow range of values ($1.15 \leqslant v_{rd} \leqslant 1.30$) for which useful triple-discontinuity solutions exist for a VDW fluid. Indeed, for slightly positive values of δ_3 and δ_4 these solutions do exist in the sense that

$$s_{r3} > s_{r4}, \quad s_{r2} > s_{r1}, \quad M_3 < 1 < M_4, \quad p_{r3}/p_{r4} < 1 < p_{r2}/p_{r1}. \tag{3.21}$$

As v_{rd} approaches v_{rd}^* from below, both shocks weaken. It is experimentally advantageous, therefore, to choose state d as close to the coexistence curve as possible. This choice must be made such that state 4 does not enter a two-phase flow regime nor come near the critical point. For a sufficiently large m value, with v_{rd} in the above range, and with δ_3 and δ_4 restricted to values such that $v_{ra} < v_{r4} < v_{rd} < v_{r3} < v_{rb}$ the foregoing global construction demonstrates that triple-discontinuity solutions exist.

Satisfactory results, in terms of an experimentally detectable value for p_{r3}/p_{r4} are

https://doi.org/10.1017/S0022112001005444 Published online by Cambridge University Press

Case	State	p_r	v_r	Γ	M
MH1	1	0.8666	2.4597	0.2258	1.0097
	2	0.9282	2.0931	0.0822	0.9863
	3	0.9282	1.9600	−0.0914	0.9793
	4	0.9866	1.5733	−0.0780	1.0108
MH2	1	0.7549	3.2617	0.4770	1.0527
	2	0.8807	2.4479	0.2620	0.9476
	3	0.8807	2.2627	0.0685	0.9805
	4	1.0056	1.4432	0.1886	1.0127

TABLE 2. Shock tube conditions for MH1 and MH2 for $v_{rd} = 1.67$.

Case	v_{rd}	Γ_d	δ_3	δ_4
VDW1	1.20	−1.0503	0.506	0.145
VDW2	1.20	−1.0503	0.305	0.043
MH1	1.67	−0.1499	0.395	0.214
MH2	1.67	−0.1499	0.089	0.083

TABLE 3. Sample input conditions for fluid FC-70.

obtained with state d close to the coexistence curve. With appropriate choices for δ_3 and δ_4, Γ_3 and Γ_4 are positive as shown in figures 4(b) and 5(b), and tables 1 and 2. It is therefore not necessary for either of these values to be negative. This may be important for experimentally demonstrating a RSW since it maximizes the pressure jump across both shocks. Of course, it is essential that the adiabat curve that connects these states pass through the negative-Γ region as shown.

When applied to commercially available fluids, the outlined procedure yields encouraging results for realizable experiments. Table 3 provides fluid properties and shock tube initial conditions for FC-70. Since shock tube experiments, based on the theory just developed, are to be performed with FC-70, it is imperative that the above analysis be confirmed with a more realistic EOS. Figure 5 illustrates the shock tube initial conditions for FC-70 using the MH EOS for the data in table 3. In both MH cases state d is a vapour state well removed from the critical point. Compared to the VDW results, the negative-Γ region is noticeably smaller and further removed from the critical point, thus the region of initial conditions is significantly reduced. The wave fields generated using the MH EOS also contain discontinuities of comparatively reduced strength as represented by the respective pressure ratios. Note that a smaller value for the pressure ratio p_{r3}/p_{r4} corresponds to a stronger RSW. The maximum-strength RSW, for a given value of v_{rd}, is determined by the ratio p_b/p_a and table 4 indicates that any RSW will be weak, but some should be experimentally detectable. For the VDW simulations, the RSW pressure ratio is $p_{r3}/p_{r4} = 0.9053$ for case VDW1 and $p_{r3}/p_{r4} = 0.8256$ for case VDW2. Compared to these representative cases, the RSW pressure ratio for the MH simulations is increased somewhat with $p_{r3}/p_{r4} = 0.9408$ for case MH1 and $p_{r3}/p_{r4} = 0.8758$ for case MH2.

Several general characteristics for triple-discontinuity solutions are evident from the shock tube flow modelling. A narrow, but finite, range of v_{rd} values yield flows with three distinct discontinuities. In terms of experimental feasibility, the incident waves are predicted to have sufficient strength (in terms of pressure ratios) to be detected with readily available pressure transducers. As is typical of non-classical dense gas

https://doi.org/10.1017/S0022112001005444 Published online by Cambridge University Press

Case	p_{r2}/p_{r1}	T_{r2}/T_{r1}	p_{r3}/p_{r4}	T_{r3}/T_{r4}
VDW1	1.1288	1.0024	0.9053	0.9959
VDW2	1.2697	1.0037	0.8256	0.9923
MH1	1.0710	1.0021	0.9408	0.9966
MH2	1.1666	1.0033	0.8758	0.9932

TABLE 4. Ratios for table 3 cases.

flows, the shock Mach numbers are close to unity. For each of the four cases presented, the largest flow speed is $u_1 = 63.35\,\mathrm{m\,s^{-1}}$, the speed of the compression shock wave propagating at $M_1 = 1.0291$ in case VDW2.

4. Computational modelling

The two-dimensional Euler equations are numerically integrated for the wave field evolution. In non-dimensional conservative-vector form,

$$\frac{\partial \boldsymbol{Q}}{\partial t} + \frac{\partial \boldsymbol{E}}{\partial x} + \frac{\partial \boldsymbol{F}}{\partial y} = 0, \tag{4.1}$$

$$\boldsymbol{Q} = [\rho_r, \rho_r u, \rho_r v, \rho_r e_t]^T, \tag{4.2}$$

$$\boldsymbol{E} = [\rho_r u, \rho_r u^2 + Z_c p_r, \rho_r uv, u(e_t + Z_c p_r)]^T, \tag{4.3}$$

$$\boldsymbol{F} = [\rho_r v, \rho_r uv, \rho_r v^2 + Z_c p_r, v(e_t + Z_c p_r)]^T. \tag{4.4}$$

Here, time is denoted by t, x and y are the axial and transverse spatial coordinates with u and v the velocity components in the respective coordinate directions, e_t is the specific total energy, and Z_c is the critical compressibility. The density ρ and pressure p are again written in reduced form denoted by the r subscript. The overall non-dimensionalization scheme is as follows:

$$\left.\begin{array}{lll} p_r = \bar{p}/\bar{p}_c, & \rho_r = \bar{\rho}/\bar{\rho}_c, & T_r = \bar{T}/\bar{T}_c, \\ u = \bar{u}/(\bar{R}\bar{T}_c)^{1/2}, & v = \bar{v}/(\bar{R}\bar{T}_c)^{1/2}, & e = (\bar{e} - e_c)/(\bar{R}\bar{T}_c)^{1/2}, \\ s = (\bar{s} - \bar{s}_c)/\bar{R}, & a = \bar{a}/(\bar{R}\bar{T}_c)^{1/2}, & x = \bar{x}/\bar{L}, y = \bar{y}/\bar{L}, \end{array}\right\} \tag{4.5}$$

where the overbar and c subscript again refer dimensional quantities and critical values respectively. The characteristic dimension of the computational domain in the transverse direction is $\bar{L}$.

With $v_r = 1/\rho_r$, the VDW and MH thermal EOS are, respectively,

$$p_r = \frac{8T_r}{3v_r - 1} - \frac{3}{v_r^2}, \tag{4.6}$$

$$p_r = \frac{T_r}{Z_c(v_r - b)} + \frac{A_2 + B_2 T_r + C_2 e^{-5.475T_r}}{(v_r - b)^2} + \frac{A_3 + B_3 T_r + C_3 e^{-5.475T_r}}{(v_r - b)^3} + \frac{A_4}{(v_r - b)^4} + \frac{B_5 T_r + C_5 e^{-5.475T_r}}{(v_r - b)^5}. \tag{4.7}$$

For the VDW cases, $Z_c = 3/8$. The coefficients A_i, B_i and C_i are numerical constants found in Martin & Hou (1955, 1959) with useful estimation techniques for the Boyle

https://doi.org/10.1017/S0022112001005444 Published online by Cambridge University Press

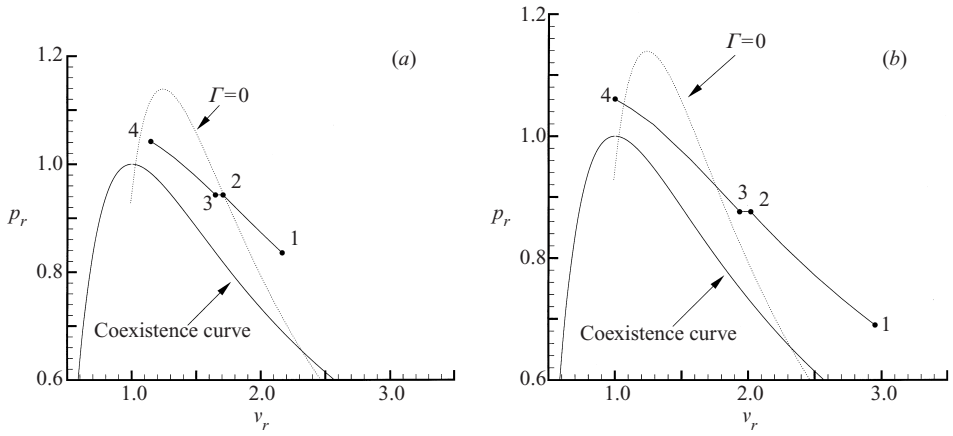


FIGURE 7. p_r, v_r diagrams showing the coexistence curve and $\Gamma = 0$ contour with states 1–4 for cases (*a*) VDW1 and (*b*) VDW2.

temperature and acentric factor given by Cramer (1989) and Cramer & Best (1991). Expressions for flow variables such as speed of sound, enthalpy, and entropy can be calculated according to Cramer (1989) for both EOS.

The Euler simulations are computed using the explicit, total variation diminishing predictor-corrector (TVDPC) scheme of Brown & Argrow (1997, 1998). The scheme is second-order accurate in space and time. Adiabatic solid-wall boundary conditions are imposed. Validation of the numerical algorithm for VDW and MH calculations is shown in Brown & Argrow (1997).

5. Simulations

The shock tube is modelled as a 5.0 m × 0.025 m plane with solid-wall boundary conditions. The computational domain is divided into 2000 cells in the x-direction along the length of the tube and 40 cells in the transverse y-direction. The CFL number for all Euler simulations is 0.4. Thermodynamic properties of FC-70 used for the simulations are

$$\bar{p}_c = 10.2\,\text{atm}, \quad \bar{T}_c = 608.2\,\text{K}, \quad \bar{M} = 821\,\text{kg kmol}^{-1}, \quad m = 118.7$$

where $\bar{M}$ is the molecular weight.

Four cases are presented to test the validity of the initial-condition algorithm for generating a triple-discontinuity wave field. These cases represent possible initial conditions for experiments. Figures 7 and 8 show the VDW and MH (p_r, v_r)-planes for FC-70 first shown in figures 4 and 5, but now with the thermodynamic states from the Euler simulations superimposed. The closely spaced points that appear as curves connecting states 1–4 are the discrete p_r, v_r states of each of the 2000 computational cells. The curve between states 3 and 4 represents the corresponding RSW adiabat, with the CSW adiabat between states 1 and 2. The line between states 2 and 3 is the isobaric solution for the CS. Note that these thermodynamic states are associated with the incident wave field and do not change until the waves reflect from the endwalls. Particular thermodynamic values associated with states 1–4 are in tables 1 and 2. For an 'ideal' Euler calculation, there are no intermediate states through discontinuities. Because the 'numerical discontinuities' are smeared by the shock-capturing scheme, there is an artificial shock profile with associated thermodynamic

https://doi.org/10.1017/S0022112001005444 Published online by Cambridge University Press

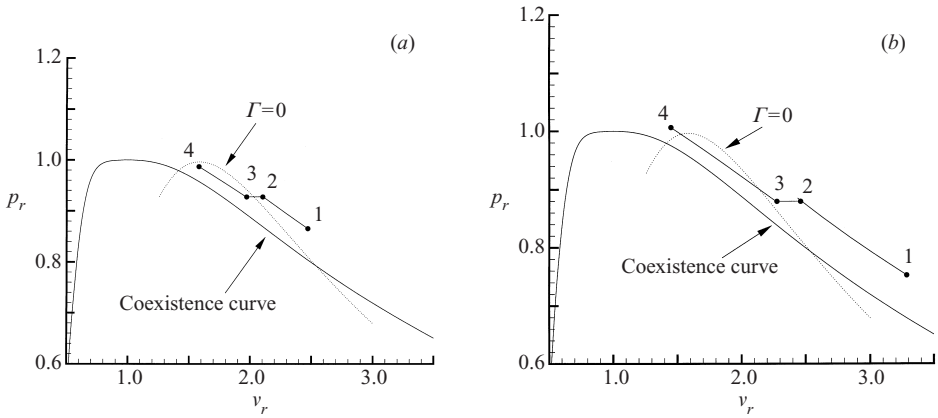


FIGURE 8. p_r, v_r diagrams showing the coexistence curve and $\Gamma = 0$ contour with states 1–4 for cases (*a*) MH1 and (*b*) MH2.

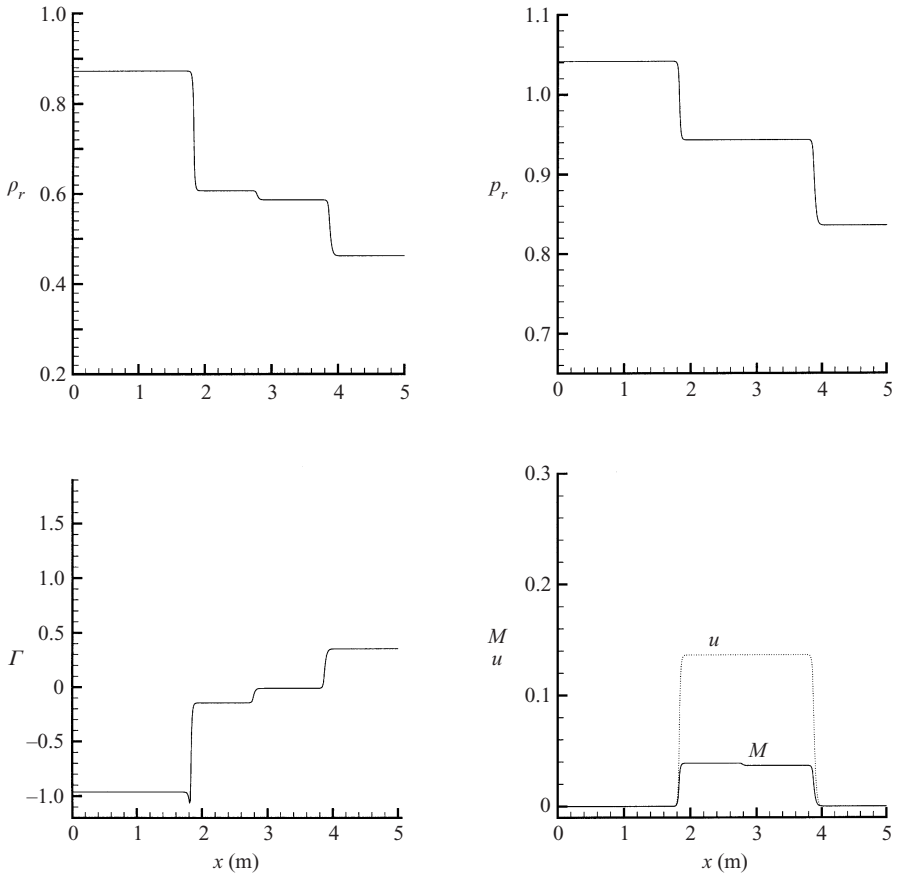


FIGURE 9. Distribution of p_r, ρ_r, u, M and Γ for case VDW1.

states. This simulation feature is discussed by Argrow (1996). The agreement between the flow states computed with the analytic procedure and the simulated states is excellent for all cases.

Figures 9–12 verify the triple-discontinuity characteristics of each case. The centre-

https://doi.org/10.1017/S0022112001005444 Published online by Cambridge University Press

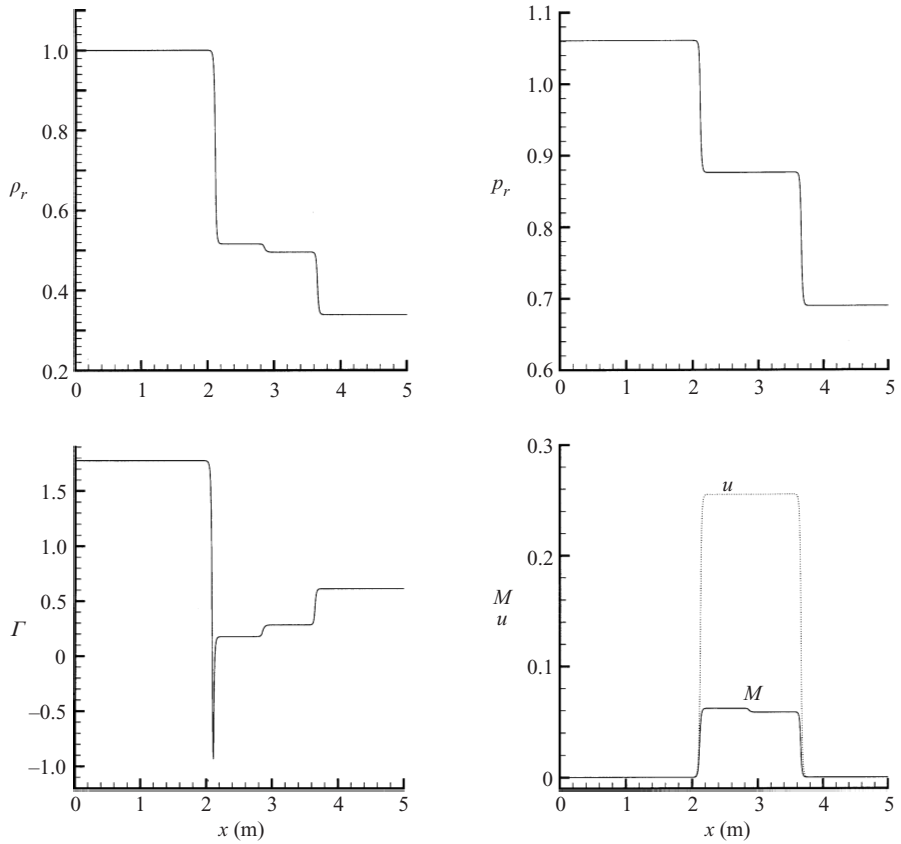


FIGURE 10. Distribution of p_r, ρ_r, u, M and Γ for case VDW2.

line distributions of p_r, ρ_r, u, M, and Γ correspond to the p_r, v_r mappings in figures 7 and 8. The flow velocity u and Mach number M are with respect to a laboratory frame. This is in contrast to tables 1 and 2 where M is measured relative to the shock-fixed coordinates of the appropriate shock. The triple-discontinuity solution is most evident in the centreline density profile. The left-moving RSW and the right-moving CSW correspond to the large jumps in ρ_r and the CS corresponds to the smaller jump between them. The apparent undershoot in the Γ-distribution is again associated with the smearing of the numerical discontinuity described by Argrow (1996). Both the RSW and CSW have relatively low propagation speeds in all cases. For instance, the CSW in case MH2 attains a speed of only $52.61\,\mathrm{m\,s^{-1}}$ compared to $23.12\,\mathrm{m\,s^{-1}}$ for the RSW. The low wave-propagation speeds are due to the relatively low speed of sound typical of a dense gas.

An interesting feature of the VDW2 and MH2 cases is an apparent relaxation of the $\Gamma < 0$ condition for negative nonlinearity. Evidently, it was assumed that all wave states must lie within the $\Gamma < 0$ region to produce a RSW. For the VDW2 and MH2 initial conditions, a RSW is produced even though states 3 and 4 are both outside the $\Gamma < 0$ region. This relaxation of the $\Gamma < 0$ restriction follows from the requirement that states 3 and 4 lie between states a and b. Since states a and b define the Rayleigh line for a double-sonic RSW adiabat (see figure 6), states 3 and 4 must constitute a single wave, regardless of the respective values of Γ. By placing states 3 and 4 to satisfy this condition, the Rayleigh line defining the discontinuity must begin at state

https://doi.org/10.1017/S0022112001005444 Published online by Cambridge University Press

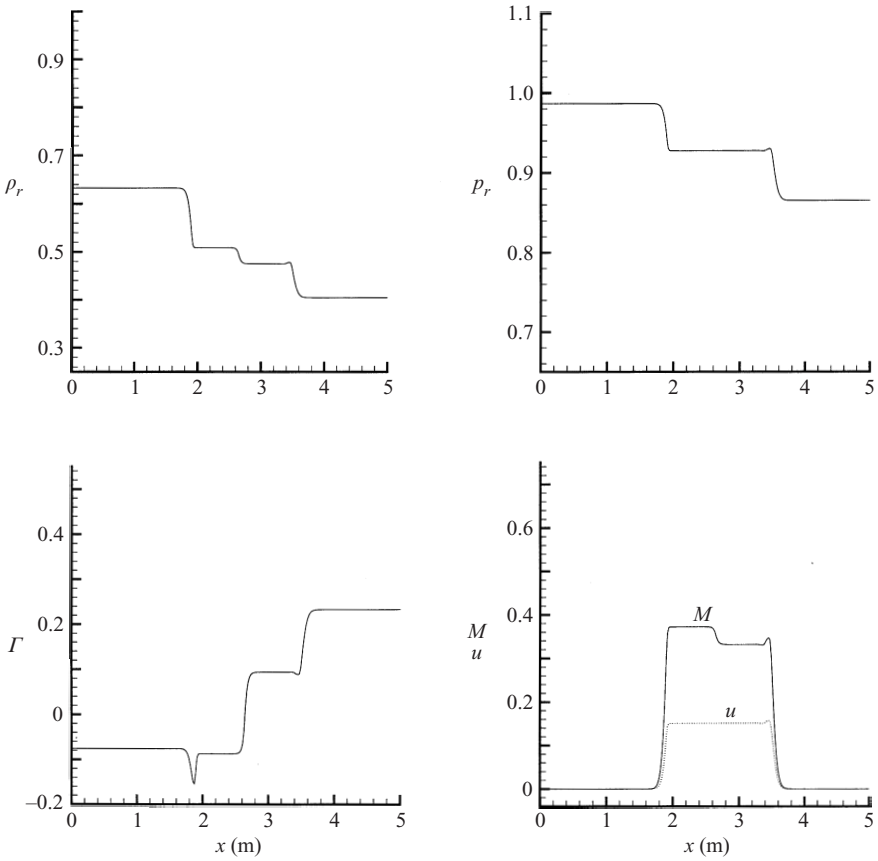


FIGURE 11. Distribution of p_r, ρ_r, u, M and Γ for case MH1.

4, pass within the $\Gamma < 0$ region, and not cross the adiabat before reaching state 3. This guarantees the discontinuity will not be a composite wave and indeed is a single RSW.

6. Summary

A review of the literature reveals only one experimental study (Borisov *et al.* 1983) that focuses upon single-phase, non-classical dense gas phenomena. The interpretation of the results of that study is inconsistent with the thermodynamic requirements for non-classical behaviour. The range of F-13 thermodynamic states in the rarefaction wave they describe indicates that some of these states are possibly in the vapour–liquid mixture region. The apparent non-classical features of the wave may be associated with critical point phenomena or two-phase flow. This conclusion is consistent with that of others (Thompson 1991; Kutateladze *et al.* 1987; Cramer & Sen 1986).

In preparation for a new experimental study, a global model is constructed to investigate the initial conditions required to produce a triple-discontinuity wave field in the incident flow of a shock tube, where one discontinuity is a RSW. The described procedure provides a starting point for shock tube experiments that produce non-classical phenomena due to negative nonlinearity in the vapour phase of dense fluids. For a given experiment, the flow field initial conditions are fixed with the choice

https://doi.org/10.1017/S0022112001005444 Published online by Cambridge University Press

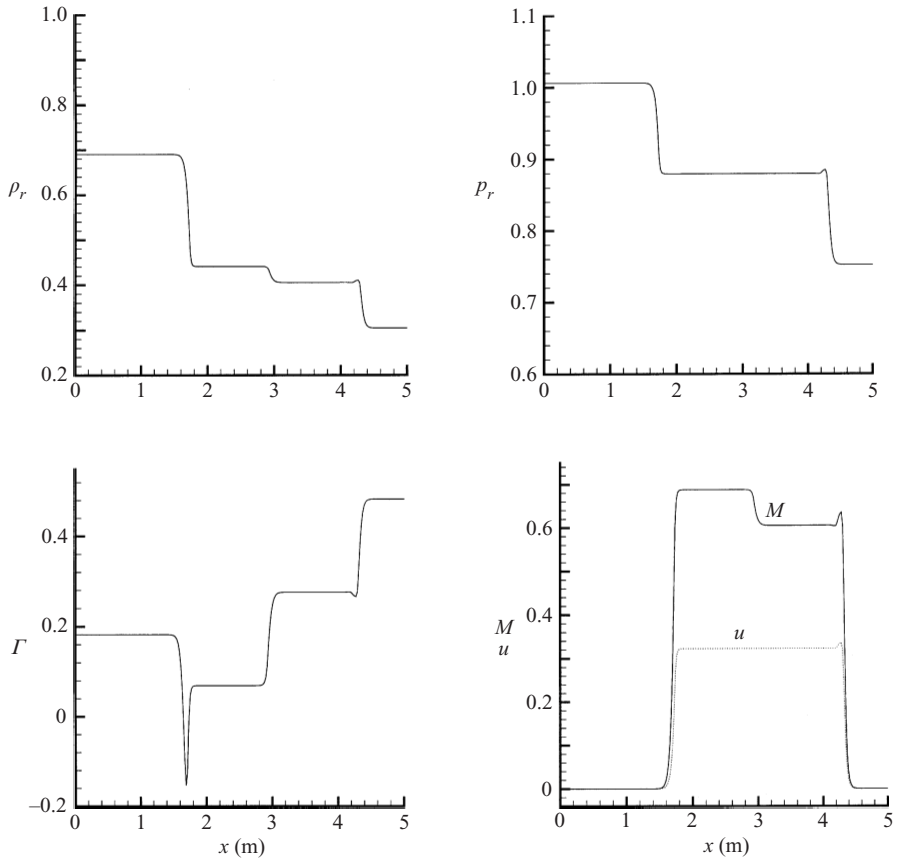


FIGURE 12. Distribution of p_r, ρ_r, u, M and Γ for case MH2.

of three parameters: v_{rd}, δ_3, and δ_4. Adjustment of the input parameters enables an approximate maximization of the RSW shock strength, thus enhancing the probability of detection. For the fluid FC-70, a finite but small region of initial states exists where the entropy jump and upstream Mach number are satisfactory. The VDW model is confirmed using a similar model with the MH EOS. This model further demonstrates that the high-pressure state is not close to either the critical point or the coexistence curve. Further analysis of the FC-70 wave field, using an Euler flow solver with the MH EOS, provides additional confirmation of the global model.

There are initial conditions that produce a RSW for which the upstream state 4 and the downstream state 3 have Γ-values greater than zero. This unexpected prediction from the conceptual model is verified with the Euler flow solver and indicates that some conditions previously thought to produce a composite rarefaction wave (shock–fan–shock) actually produce a single RSW. By locating states 4 and 3 between the tangency points of the Rayleigh line on the shock adiabat (figure 6), the resulting wave is a RSW with no composite features. This relaxation of initial conditions may be fortuitous for proposed experiments, since any increase in the pressure differentials should make the wave field easier to resolve.

This work is supported, in part, by NSF Grant CTS-9902126.

https://doi.org/10.1017/S0022112001005444 Published online by Cambridge University Press

Appendix. Equations for a van der Waals Fluid

$$p_r = \frac{8T_r}{3v_r - 1} - \frac{3}{v_r^2}, \tag{A 1}$$

$$h_r = \text{enthalpy} = \frac{\bar{h} - \bar{h}_c}{\bar{R}\bar{T}_c} = \frac{3(v_r - 3)}{4v_r} + \frac{3v_r T_r}{3v_r - 1} + m(T_r - 1), \tag{A 2}$$

$$s_r = \text{entropy} = \frac{\bar{s} - \bar{s}_c}{\bar{R}} = \ln\left(\frac{3v_r - 1}{2}\right) + m \ln T_r, \tag{A 3}$$

$$a_r = \text{speed of sound} = \frac{\bar{a}}{\bar{a}_c} = \left\{ m v_r^2 \left[\frac{m+1}{m} \frac{9T_r}{(3v_r - 1)^2} - \frac{1}{v_r^2} \right] \right\}^{1/2}, \tag{A 4}$$

$$\bar{a}_c = \frac{3}{2}\left(\frac{\bar{R}\bar{T}_c}{m}\right)^{1/2}, \tag{A 5}$$

$$\Gamma = \frac{3m}{2v_r a_r^2} \left[\frac{4(m+1)(2m+1)}{m^2} \frac{v_r^4 T_r}{(3v_r - 1)^3} - 1 \right], \tag{A 6}$$

$$T_r = \frac{(3v_{rg} - 1)(3v_{rf} - 1)(v_{rg} + v_{rf})}{8 v_{rg}^2 v_{rf}^2}, \tag{A 7}$$

$$\ln \frac{3v_{rg} - 1}{3v_{rf} - 1} = \frac{3(v_{rg} - v_{rf})(6v_{rg}v_{rf} - v_{rg} - v_{rf})}{(3v_{rg} - 1)(3v_{rf} - 1)(v_{rf} + v_{rg})}. \tag{A 8}$$

REFERENCES

Argrow, B. M. 1996 Computational analysis of dense gas shock tube flow. *Shock Waves* **6**, 241–248.

Borisov, A. A., Borisov, A. L., Kutateladze, S. S. & Nakoryakov, V. E. 1983 Rarefaction shock wave near the thermodynamic critical point. *J. Fluid Mech.* **126**, 59–73.

Brown, B. P. & Argrow, B. M. 1997 Two-dimensional shock tube flow for dense gases. *J. Fluid Mech.* **349**, 95–115.

Brown, B. P. & Argrow, B. M. 1998 Nonclassical dense gas flows for simple geometries. *AIAA J.* **36**, 1842–1847.

Brown, B. P. & Argrow, B. M. 2000 Application of bethe-zel'dovich-thompson fluids in organic rankine cycle engines. *J. Propulsion Power* **16**, 1118–1124.

Cramer, M. S. 1989 Shock splitting in single-phase gases. *J. Fluid Mech.* **199**, 281–296.

Cramer, M. S. 1991 Nonclassical dynamics of classical gases. In *Nonlinear Waves in Real Fluids*, pp. 91–145. Springer.

Cramer, M. S. & Best, L. M. 1991 Steady, isentropic flows of dense gases. *Phys. Fluids* A **3**, 219–226.

Cramer, M. S. & Sen, R. 1986 Shock formation in fluids having embedded regions of negative nonlinearity. *Phys. Fluids* **29**, 2181–2191.

Cramer, M. S. & Sen, R. 1987 Exact solutions for sonic shocks in van der waal's gases. *Phys. Fluids* **30**, 377–385.

Cramer, M. S. & Sen, R. 1990 Mixed nonlinearity and double shocks in superfluid helium. *J. Fluid Mech.* **221**, 233–261.

Emanuel, G. 1996 Analysis of a critical point with application to fluid mechanics. Internal report AME Report 96–1. University of Oklahoma, Norman, OK.

Emanuel, G. 1997 Thermodynamics assessment of the non-classical region. Internal report AME Report 97–1. University of Oklahoma, Norman, OK.

Kutateladze, S. S., Nakoryakov, V. E. & Borisov, A. A. 1987 Rarefaction waves in liquid and gas-liquid media. *Ann. Rev. of Fluid Mech.* **19**, 577–600.

https://doi.org/10.1017/S0022112001005444 Published online by Cambridge University Press

Martin, J. J. & Hou, Y. C. 1955 Development of an equation of state for gases. *Am. Inst. Chem. Engng J.* **5** (2), 142–151.

Martin, J. J. & Hou, Y. C. 1959 An improved equation of state for gases. *Am. Inst. Chem. Engng J.* **5** (2), 142–151.

Stewart, R. B., Jacobsen, R. T. & Penocello, S. G. 1969 *ASHRAE Thermodynamic Properties of Refrigerants*. American Society of Heating, Refrigerating, and Air-Conditioning Engineers.

Thompson, P. A. 1988 *Compressilbe Fluid Dynamics*. McGraw-Hill.

Thompson, P. A. 1991 Liquid-vapor adiabatic phase changes and related phenomena. In *Nonlinear Waves in Real Fluids* (ed. A. Kluwick), pp. 147–213. Springer.

Thompson, P. A., Carofano, G. A. & Kim, Y. 1986 Shock waves and phase changes in a large heat capacity fluid emerging from a tube. *J. Fluid Mech.* **166**, 57–96.

Thompson, P. A. & Kim, Y. 1983 Direct observation of shock splitting in a vapor-liquid system. *Phys. Fluids* **26**, 3211–3215.

Thompson, P. A. & Lambrakis, K. C. 1973 Negative shock waves. *J. Fluid Mech.* **60**, 187–208.

https://doi.org/10.1017/S0022112001005444 Published online by Cambridge University Press